Earthq Eng & Eng Vib (2023) 22: 965-977 **DOI**: https://doi.org/10.1007/s11803-023-2214-8

Seismic fragility analysis of clay-pile-pier systems considering the optimization of ground motion intensity measures

Zhang Panpan†, Zhang Lei‡ and Zhang Zhen§

School of Civil Engineering and Architecture, Wuhan University of Technology, Wuhan 430070, China

Abstract: The performance of clay-pile-pier system under earthquake shaking was comprehensively examined via three-dimensional finite element analyses, in which the complex stress-strain relationships of a clay and piled pier system were depicted by a hyperbolic-hysteretic and an equivalent elastoplastic model, respectively. One hundred twenty ground motions with varying peak accelerations were considered, along with the variations in bridge superstructure mass and pile flexural rigidity. Comprehensive comparison studies suggested that peak pile-cap acceleration and peak pile-cap velocity are the optimal ground motion intensity measures for seismic responses of the pier and the pile, respectively. Furthermore, based on two optimal ground motion intensity measures and using curvature ductility to quantify different damage states, seismic fragility analyses were performed. The pier generally had no evident damage except when the bridge girder mass was equal to 960 t, which seemed to be comparatively insensitive to the varying pile flexural rigidity. In comparison, the pile was found to be more vulnerable to seismic damage and its failure probabilities tended to clearly reduce with the increment of pile flexural rigidity, while the influence of the bridge girder mass was relatively minor.

Keywords: clay-pile-pier system; seismic fragility analysis; ground motion; intensity measures; damage probability

1 Introduction

Many coastal areas worldwide are distributed with a large range of thick soft clay strata, where numerous structures such as bridges and wind turbines are supported by pile foundations. A pile-pier system is widely employed in bridge engineering because of its high bearing capacity, low settlement and convenient construction. However, many post-earthquake investigations have indicated that piled bridges embedded in soft clay or liquefiable soils are susceptible to seismic failures (Boulanger *et al*., 1999; Bhattacharya *et al*., 2014; Mylonakis *et al*., 2006; Mohanty *et al*., 2021; Tang *et al*., 2010), which are mainly due to the earthquake-induced damage to the pile-pier systems rather than to the bridge superstructures.

A number of seismic model tests including 1-g shaking table (Meymand, 1998; Saha *et al*., 2015) and high-g centrifuge tests (Banerjee *et al*., 2014; Li *et al*., 2022; Yang and Yang, 2016; Yang *et al*., 2019; Zhang *et al*., 2017b, 2022) have been carried out to explore the seismic response of piled structures built in clayey ground or saturated sand. Alternatively, numerical approaches such as finite element (FE) analysis have been favorably utilized to study the seismic behavior of soil-pile-structure systems (Azizkandi *et al*., 2018; Banerjee *et al*., 2014; Dehghanpoor *et al*., 2019; Maheshwari *et al*., 2004; Tang *et al*., 2016; Zhang and Liu, 2017). Most of these studies focused on the bending moment response of the pile and acceleration responses at various locations, subjected to various ground motions; however, the seismic damage evaluation of a piled structure system was generally not considered, especially for those installed in soft clays. Given the significant randomness and uncertainty of earthquakes, the seismic performance of a structure against seismic risk cannot be fully evaluated by performing the seismic analysis employing few ground motions without reasonable variations in both the frequency content and shaking intensity. By employing a relatively large amount of representative ground motions, seismic fragility analysis can quantitatively reflect the seismic safety performance of a structure at various ground motion intensities, which has been widely adopted to evaluate the safety of bridge structures against seismic risks (Hwang *et al*., 2000; Tavares *et al*., 2013; Wang *et al*. 2012; Zhang *et al*., 2008). To perform seismic fragility analysis, a better selection of ground motion intensity measures can effectively reduce the uncertainty

Correspondence to: Zhang Lei, School of Civil Engineering and Architecture, Wuhan University of Technology, Wuhan 430070, China
Tel: +86-18827009754
E-mail: zhangleigeo@whut.edu.cn
†PhD Candidate; ‡Associate Professor; §Master Student

Supported by: National Natural Science Foundation of China under Grant Nos. 52178353, 51808421 and the Fundamental Research Funds for the Central Universities (WUT: 2020III043)
Received January 13, 2022; **Accepted** August 4, 2022

in predicting structure damage (Song *et al*., 2019; Yang *et al*., 2015; Yakhchalian *et al*., 2015). Peak ground acceleration (PGA) is normally used as the ground motion intensity measure (Chen *et al*., 2022; Padgett *et al*., 2008; Shafieezadeh *et al*., 2012; Tang and Chen, 2020; Zhong *et al*., 2016). However, as observed in previous studies (Zhong *et al*., 2019), likely due to the complex seismic soil-structure interaction effect, PGA is not always a convincing ground motion intensity measure when different soil-structure systems are considered. In fact, some other ground motion intensity measures, such as peak ground velocity (PGV) (Zelaschi *et al*., 2019), peak ground displacement (PGD) (Wu *et al*., 2021) and velocity spectrum intensity (VSI) (Bradley *et al*., 2009), have been proposed for assessing the effect of ground motion intensity on different soil-structure systems.

In the present study, to comprehensively explore the seismic safety of a piled pier structure embedded in clayey ground, a series of dynamic FE analyses were performed employing 120 realistic ground motions, considering the variations in both pile flexural rigidity and bridge girder mass. The complex stress-strain relationships of soft clay and the piled pier system under earthquake loadings were depicted using hyperbolic-hysteretic and equivalent elastic–perfectly plastic models, respectively. Comparison analyses were performed to attain the respective optimal seismic ground motion intensity measures to correlate with the seismic damage extents of both the pier and the pile. Furthermore, a suite of seismic fragility curves for the pier and pile were obtained with respect to various damage states, which could be employed to preliminarily assess the seismic safety of a similar clay-pile-pier system.

2 Finite element modeling program

2.1 Basic information

The geometric model adopted in this study is mainly composed of a pier, a lumped mass (or termed added mass), a pile cap, and a 2×2 pile group embedded in soft clay stratum. As Fig. 1 shows, considering that the soft clay-pile-pier system is geometrically symmetrical to the earthquake shaking direction, a half three-dimensional (3D) FE model for the system is established, which includes 13,422 solid hexahedron elements and 103 beam elements. The system is considered overlying a rigid bedrock, and the normal directions of two vertical faces in parallel with the shaking direction are constrained. In addition, two faces perpendicular to the ground motion direction were tied to ensure that nodes at the same elevations have consistent motions, which was also used in other studies (Banerjee *et al*., 2014; Tsinidis *et al*., 2016) to simulate a free-field ground motion condition.

2.2 Soil constitutive model

Normally consolidated clayey ground is considered in the present study, and its basic properties are provided in Table 1. As demonstrated in Fig. 2, the dynamic behavior of soft clay is depicted utilizing a hyperbolic-hysteretic constitutive model that was initially established by Banerjee *et al*. (2014). The nonlinear stress-strain relationships for this clay model in initial loading, unloading, and reloading stages can be expressed by Eqs. (1)–(3).

$$q = q_{\mathrm{f}} - \left(\frac{q_{\mathrm{f}}}{1 + 3G_{\max}\varepsilon_{\mathrm{s}} / q_{\mathrm{f}}} \right) \tag{1}$$

$$q = -2q_{\mathrm{f}} + \left[\frac{2q_{\mathrm{f}}}{1 + 3G_{\max}\left(\varepsilon_{\mathrm{r1}} - \varepsilon_{\mathrm{s}}\right) / 2q_{\mathrm{f}}} \right] + q_{\mathrm{r1}} \tag{2}$$

$$q = 2q_{\mathrm{f}} - \left[\frac{2q_{\mathrm{f}}}{1 + 3G_{\max}\left(\varepsilon_{\mathrm{s}} - \varepsilon_{\mathrm{r2}}\right) / 2q_{\mathrm{f}}} \right] - q_{\mathrm{r2}} \tag{3}$$

where ε_{s} and q are, respectively, the generalized shear strain and current deviator stress; $\varepsilon_{\mathrm{r1}}$ and $\varepsilon_{\mathrm{r2}}$ are the generalized shear strains at the two reversal points; q_{r1} and q_{r2} are, respectively, the deviator stresses at the two

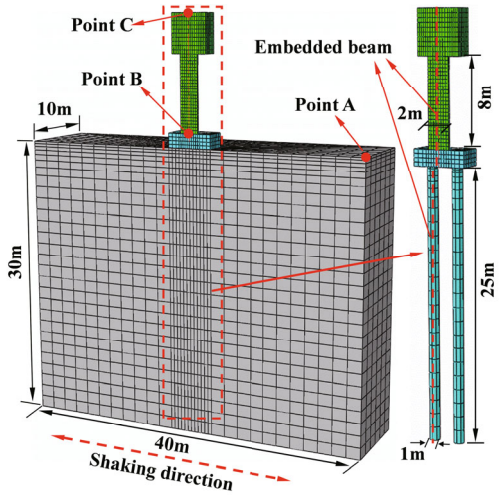

Fig. 1 Finite element mesh of the half clay-pile-pier system

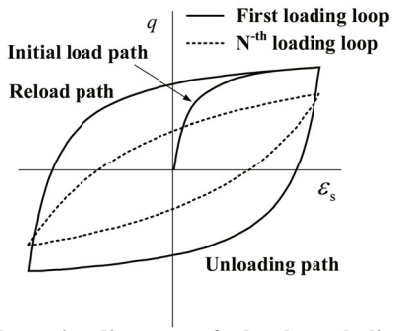

Fig. 2 Schematic diagram of the hyperbolic-hysteretic constitutive model

reversal points; q_f is the equivalent stress at failure; and G_{max} is the small-strain or maximum shear modulus.

The small-strain shear modulus and the equivalent stress at failure of soft clay can be obtained using Eqs. (4) and (5), respectively.

$$G_{max} = A(p_0')^{0.653} \tag{4}$$

$$q_f = \beta \frac{6\sin(\varphi)\, p_0'}{3 - \sin(\varphi)} \tag{5}$$

where p'_0 is the initial mean effective stress, having a unit of kPa consistent with that of G_{max}; A is the modulus correction constant, which is related to the type of soft soil; φ is the internal friction angle of clay; and β is the initial state parameter of soil, which is related to the over consolidation ratio, compression index and recompression index.

According to the relevant previous studies (Banerjee *et al*., 2014; Zhang *et al*., 2017a), parameters A and β are set as 2060 and 0.6, respectively, for normally consolidated kaolin and soft Singapore marine clays.

As Fig. 3 shows, using this hyperbolic-hysteretic soil model, the computed cyclic shear stress-strain loops compare reasonably well with that from cyclic triaxial tests conducted on normally consolidated kaolin clay (Banerjee *et al*., 2014). In addition, the performance of this soft clay model has been favorably examined with results from a series of centrifuge earthquake experiments on various clay-pile-superstructure systems (Banerjee *et al*., 2014; Zhang *et al*., 2017b).

2.3 Pile-pier system modeling

Compared to the pile cap and bridge superstructure, the pile and pier are more vulnerable to structural damage subjected to strong earthquakes; the structural damage to the pile cap and bridge superstructure are neglected in this study. Some complex models such as the concrete damaged plasticity model can be employed to depict the damage evolution of concrete (Jankowiak and Łodygowski, 2005; Drygala *et al*., 2017); however, initial trial analyses have suggested that the computational efficiency with this model is largely limited under the dynamic loading conditions. A previous study (Zhang *et al*., 2021) has indicated that, for reinforced concrete columns, adopting an equivalent yield stress the elastic-perfectly plastic model can yield comparable results as those obtained by employing concrete damaged plasticity and elastoplastic models to model the concrete and reinforcement. Therefore, the equivalent elastic-perfectly plastic model is used for both the pier and the pile made of reinforced concrete; for a reinforcement ratio of 2%, the equivalent yield stress is around 15.3 MPa as shown in Table 2. The other relevant parameters for the piled pier system are also provided in Table 2. In addition, the soil-pile interface behavior is modelled via hard-contact and penalty friction algorithms, and a Rayleigh damping of 5% is applied to the piled pier system.

Table 1 Basic parameters of the soft clay

Poisson′s ratio	Density (kg/m^3)	Internal frictional angle (°)	Small-strain/maximum modulus (kPa)
0.3	1600	23	$2060(p'_0)^{0.653}$

Note: p'_0 is the initial mean effective stress of clay, having a unit of kPa.

2.4 Input ground motions

One hundred twenty realistic earthquake records are selected from the ground motion database of the Pacific Earthquake Engineering Research Center (PEER), in which the peak accelerations range from 0.01 g to 1.22 g

Table 2 Basic properties of pile-pier system

Property	Pile cap and lumped mass	Pier and pile
Density (g/cm^3)	2.5	2.5
Elastic modulus (GPa)	30	30
Poisson′s ratio	0.2	0.2
Equivalent yield stress (MPa)	-	15.3

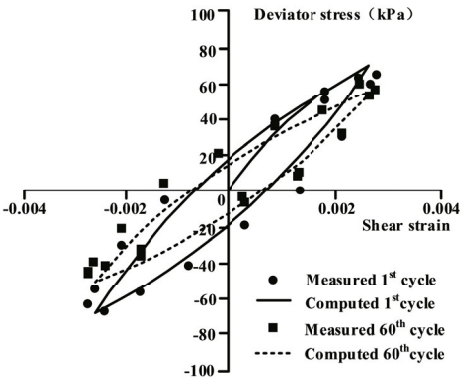

(a) γ = 0.254%

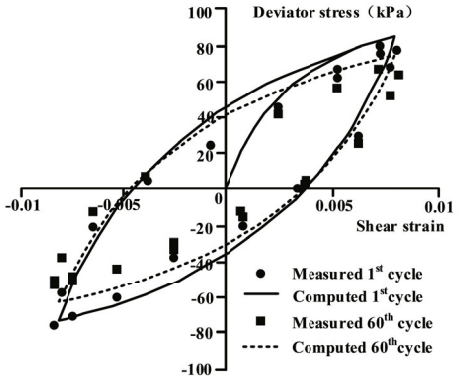

(b) γ = 0.789%

Fig. 3 Comparison of the measured and computed cyclic shear stress-strain results involving different shear strain levels

and moment magnitudes range from 5 to 8. The individual and mean spectral acceleration ratios of 120 ground motions as well as that recommended for Type IV soft ground (shear wave velocity < 150 m/s) in China′s code for seismic design of buildings (GB 50011-2010, 2010) are shown in Fig. 4, in which the spectral acceleration ratio is defined as the ratio of spectral acceleration to the corresponding peak acceleration of each earthquake record. As Fig. 4 shows, the employed earthquake records contain a wide range of seismic intensities, with the averaged response spectrum comparable to that recommended for Type IV ground in China′s seismic code (GB 50011-2010, 2010).

3 Seismic bending behavior of both pile and pier

Figure 5 plots the computed acceleration at the pile cap and the input base acceleration that was measured from the Ferndale City Hall base station during the 1960 Northern California earthquake. As can be seen from Fig. 5, the clayey ground can substantially amplify the earthquake-induced ground motion, which has also been reported in other publications (Banerjee *et al*., 2014; Mayoral *et al*., 2009; Tinawi *et al*., 1993; Zhang *et al*., 2017a).

Using the same ground motion, Figs. 6(a) and 6(b) show both the instantaneous maximum bending moment and curvature profiles for the pier and pile, respectively. As can be seen, due to the restraint effect of the pile cap, the maximum bending moments and curvatures of both pile and pier occur near the pile cap. In the subsequent parts of this study, only the maximum seismic responses of the pile and the pier are presented. Figure 7 shows the influence of ground motion intensity on the maximum pier bending moment response involving the 120 ground motions, in which two ground motion intensity measures, namely peak base acceleration (PBA) and peak pile-cap acceleration (PPA), are employed. The maximum pier bending moment gradually increases with both the increasing PBA and PPA, and the increasing trends can be well represented by two best-fit lines shown on

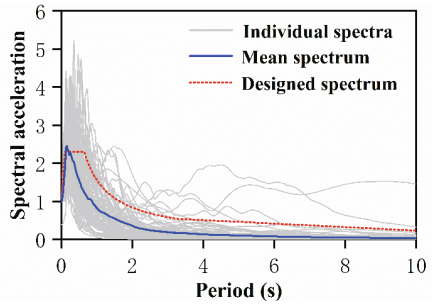

Fig. 4 Spectral acceleration ratios of the 120 ground motions and those recommended in China′s seismic code for Type IV ground (5% damping)

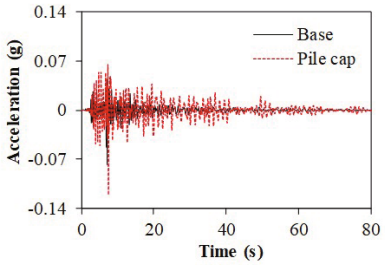

(a) Time history

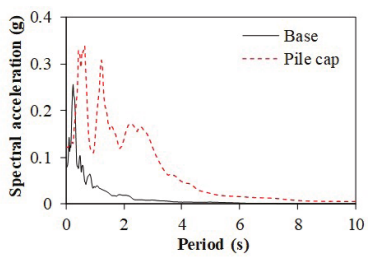

(b) Response spectrum (5% damping)

Fig. 5 Comparison between input base acceleration and those experienced at pile cap

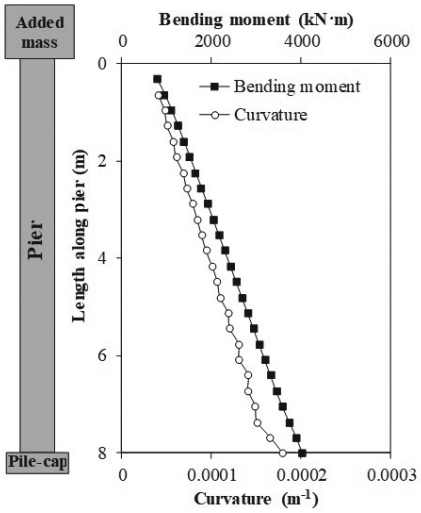

(a) Pier

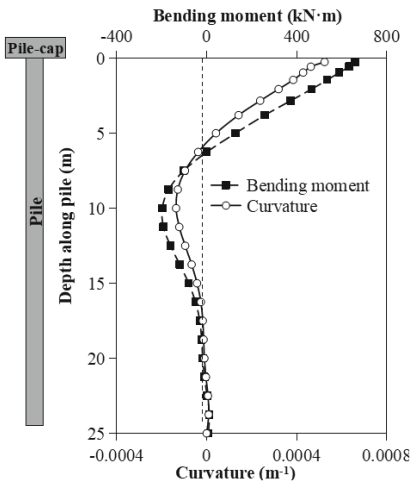

(b) Pier

Fig. 6 Profiles of maximum bending moment and curvature for both the pier and pile

Figs. 7(a) and 7(b), respectively. In addition, in comparison with the factor of PBA, the maximum pier bending moment has a more significant correlation with PPA. Similarly, as Fig. 8 shows, both PBA and peak pile-cap velocity (PPV) have an augmenting effect on the maximum response of the pile bending moment. The increasing trends are quite significant when the ground motion intensity is relatively small; for PBA larger than 0.15 g or PPV larger than 0.3 m/s, the maximum pile bending moment reaches its peak value of about 2500 kN·m and becomes almost unchanged, indicating that the pile has entered the plastic deformation domain. In addition, compared to Fig. 8(a), the best-fit line shown on Fig. 8(b) agrees much better with the data shown on the same figure, indicating that PPV is more favorable than PBA when characterizing the seismic bending moment response of the pile.

As can be concluded from the above discussions, the selection of ground motion intensity measure is important to more accurately assess the seismic performance of a piled pier system overlying soft clayey ground. In addition, once plastic deformation is introduced, the maximum bending moment response cannot reflect the seismic damage development of the piled pier system. Figure 9 presents the plot of the maximum pile curvature against PPV, suggesting that the increasing trend of maximum curvature versus PPV becomes even more significant when plastic deformation is introduced, which is significantly different from that shown in Fig. 8 for maximum bending moment response. Hence, in comparison with the maximum bending moment, the maximum curvature appears to be more capable of reflecting the damage degree of a piled pier system built in clayey ground.

4 Determination of damage states and selection of ground motion intensity measure

4.1 Determination of damage states

Various measures have been proposed to evaluate the damage states of the pile and the pier, such as curvature ductility (Brandenberg *et al*., 2011; Choi *et al*., 2004; Wang *et al*., 2019) and displacement ductility (Hwang *et al*., 2000). Following the recommendations of Choi *et al*. (2004) and Brandenberg *et al*. (2011), the curvature ductility is employed to define the damage states of the pile and the pier. Similar to that adopted in the studies of Hwang *et al*. (2000) and Wang *et al*. (2019), four different damage states, namely slight, moderate, extensive and complete damage, of both the pile and the pier are defined in this study, as listed in Table 3. As demonstrated in Fig. 10, the yield curvatures (curvature ductility equal to 1) of both the pile and the pier can be attained from the respective numerical pushover analyses, which are 0.001 m^{-1} and 0.0007 m^{-1}, respectively, in this study.

4.2 Selection of ground motion intensity measure

Given the complexity of seismic clay-pile-pier

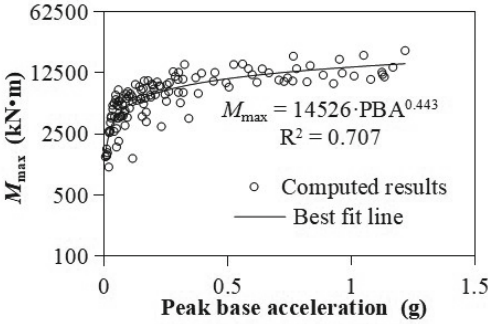

(a) Influence of peak base acceleration (PBA)

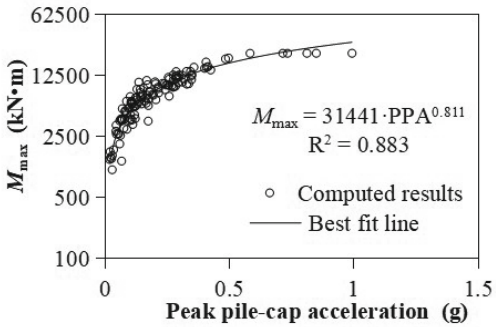

(b) Influence of peak pile-cap acceleration (PPA)

Fig. 7 Influence of ground motion intensity on the maximum pier bending moment response

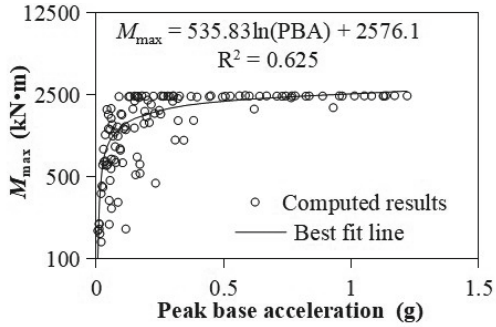

(a) Influence of peak base acceleration (PBA)

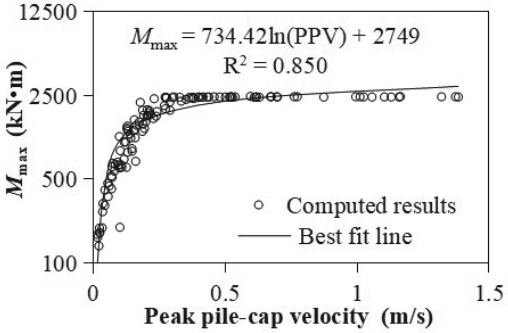

(b) Influence of peak pile-cap velocity (PPV)

Fig. 8 Influence of ground motion intensity on the maximum pile bending moment response

interaction and significant frequency-spectrum variation in ground motions, the seismic response of a pile-pier system cannot be comprehensively evaluated based on one single seismic intensity measure. The rational selection of ground motion intensity is crucial for accurately evaluating the seismic damage behavior of a structure, which also facilitates the subsequent seismic fragility analysis of the piled pier system. As shown in Table 4, with reference to the study of Riddell (2007), 16 ground motion intensity measures are employed to explore their relevance to the seismic response of the pile-pier system. These ground motion intensity measures are divided into four groups, namely acceleration-, velocity-, displacement- and spectrum-related types.

According to previous studies (Cornell *et al*., 2002), the ground motion intensity and seismic structural demand can be correlated by the following equation:

Table 3 Structure damage stage defined by curvature ductility

Damage state	Curvature ductility
Slight	$1<\upsilon<2$
Moderate	$2<\upsilon<3$
Extensive	$3<\upsilon<4$
Complete	$4<\upsilon$

Note: υ represents the curvature ductility of a structure.

$$\ln(S_{\mathrm{d}}) = b \cdot \ln(IM) + a \tag{6}$$

where S_{d} is seismic structural demand, referring to computed curvature ductility in this study; a and b are regression parameters; and IM is ground motion intensity, which can be quantified by any one of the intensity measures listed in Table 4.

The logarithmic standard deviation of the seismic structural demand can be computed using the following equation (Padgett *et al*., 2008):

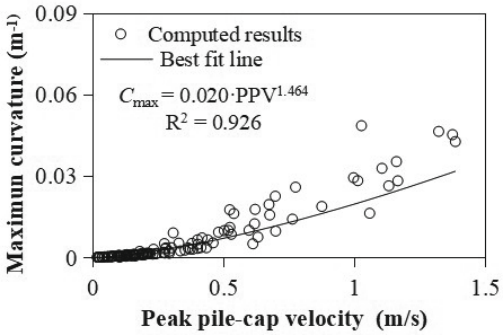

Fig. 9 Influence of PPV on the maximum curvature response of pile

Table 4 General ground motion intensity measures

Parameter	Definition	Parameter	Definition
Acceleration-related		Velocity-related	
Peak bedrock acceleration, *PBA*	$PBA = \max\lvert a(t)\rvert$	Peak bedrock velocity, *PBV*	$PBV = \max\lvert v(t)\rvert$
Peak pile-cap acceleration, *PPA*	$PPA = \max\lvert a_{\mathrm{p}}(t)\rvert$	Peak pile-cap velocity, *PPV*	$PPV = \max\lvert v_{\mathrm{p}}(t)\rvert$
Arias intensity, I_{A}	$I_{\mathrm{A}} = \frac{\pi}{2g}\int_0^{t_{\mathrm{tot}}}[a(t)]^2\mathrm{d}t$	Specific energy density, *SED*	$SED = \int_0^{t_{\mathrm{tot}}}[a(t)]^2\mathrm{d}t$
Root-mean-square acceleration, A_{rms}	$A_{\mathrm{rms}} = \sqrt{\frac{1}{t_{\mathrm{d}}}\int_{t_5}^{t_{95}} a^2(t)\mathrm{d}t}$	Root-mean-square velocity, V_{rms}	$V_{\mathrm{rms}} = \sqrt{\frac{1}{t_{\mathrm{d}}}\int_{t_5}^{t_{95}} v^2(t)\mathrm{d}t}$
Characteristic intensity, I_{C}	$I_{\mathrm{C}} = A_{\mathrm{rms}}^{1.5}\, t_{\mathrm{d}}^{0.5}$	Cumulative absolute velocity, *CAV*	$CAV = \int_0^{t_{\mathrm{tot}}}\lvert a(t)\rvert\mathrm{d}t$
Displacement-related		Spectrum-related	
Peak bedrock displacement, *PBD*	$PBD = \max\lvert u(t)\rvert$	Acceleration spectrum intensity, *ASI*	$ASI = \int_{0.1}^{0.5} S_a(T)\mathrm{d}T$
Maximum relative displacement of pile-cap, *MRPD*	$MRPD = \max\lvert u_{\mathrm{p}}(t) - u(t)\rvert$	Velocity spectrum intensity, *VSI*	$VSI = \int_{0.1}^{2.5} S_v(T)\mathrm{d}T$
Root-mean-square displacement, D_{rms}	$D_{\mathrm{rms}} = \sqrt{\frac{1}{t_{\mathrm{d}}}\int_{t_5}^{t_{95}} u^2(t)\mathrm{d}t}$	Peak spectral velocity, *PSV*	$PSV = \max\lvert S_v(T)\rvert$
Displacement intensity, I_{D}	$I_{\mathrm{D}} = \frac{\pi}{2g}\int_0^{t_{\mathrm{tot}}}[u(t)]^2\mathrm{d}t$	Peak spectral acceleration, *PSA*	$PSA = \max\lvert S_a(T)\rvert$

Note: t denotes time; t_{tot} is the duration of a ground motion; t_{d} is the effective duration of strong ground motion, where $t_{\mathrm{d}} = t_{95} - t_5$; t_5 and t_{95} are the instants corresponding to 5% and 95% of Arias intensity respectively; T is period; a and a_{p} are the bedrock and pile-cap accelerations, respectively; v and v_{p} are the bedrock and pile-cap velocities, respectively; u and u_{p} are the bedrock and pile-cap displacements, respectively; S_a and S_v are the spectral acceleration and spectral velocity, respectively.

$$\delta_{\mathrm{d}}=\sqrt{\frac{\sum_{i=1}^{N}\{\ln(S_{\mathrm{d}i})-[b\cdot\ln(IM_i)+a]\}^2}{N-2}} \tag{7}$$

where i is the ground motion number; IM_i is the ith ground motion intensity; N = 120, is the quantity of ground motions; and $S_{\mathrm{d}i}$ is the structural demand (curvature ductility) with respect to the ith ground motion.

The logarithmic standard deviations of pier curvature ductility versus ground motion intensity are presented in Fig. 11(a), in which 16 different intensity measures are involved. As can be seen, the logarithmic standard deviations associated with displacement-related intensity measures are the largest, while those involving acceleration type intensity measures are, on average, the smallest. The smaller the logarithmic standard deviation, the greater dependency the seismic structural demand has on the selected intensity measure. In addition, Fig. 11(a) suggests that the use of intensity measure PPA can lead to the least logarithmic standard deviation, which is thereby adopted as the optimal intensity measure to evaluate the seismic damage of the pier in this study. Similar plots for the pile are presented in Fig. 11(b), which indicates that PPV is the optimal intensity measure for the evaluation of seismic pile response.

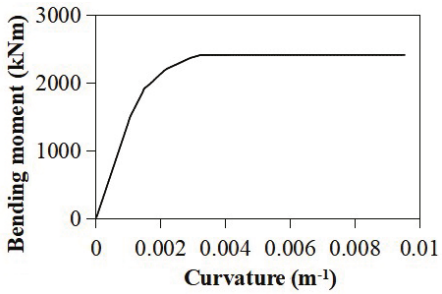

Fig. 10 Plot of pile bending moment against curvature

5 Seismic fragility analysis

A suite of further FE analyses involving the 120 ground motions and variations in the pile-pier configuration are performed. On the basis of the analysis results, as well as the four damage states and two optimal intensity measures developed in the previous

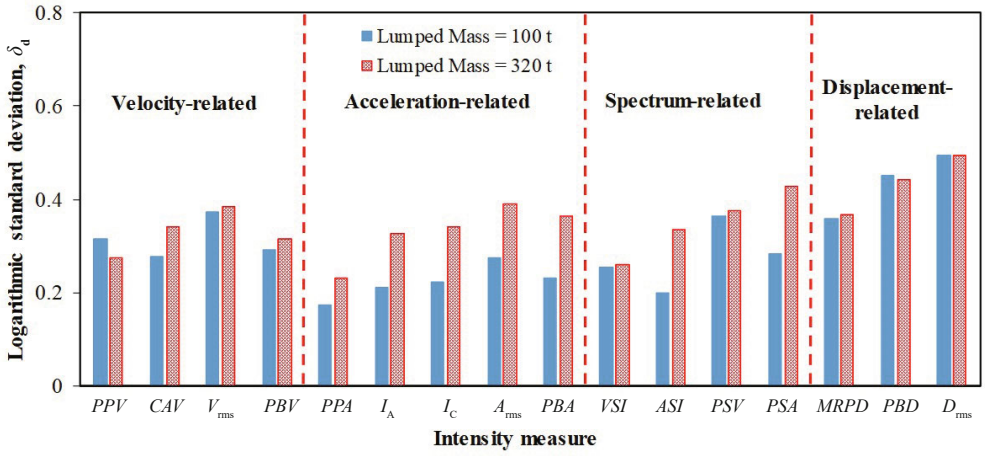

(a) Pier

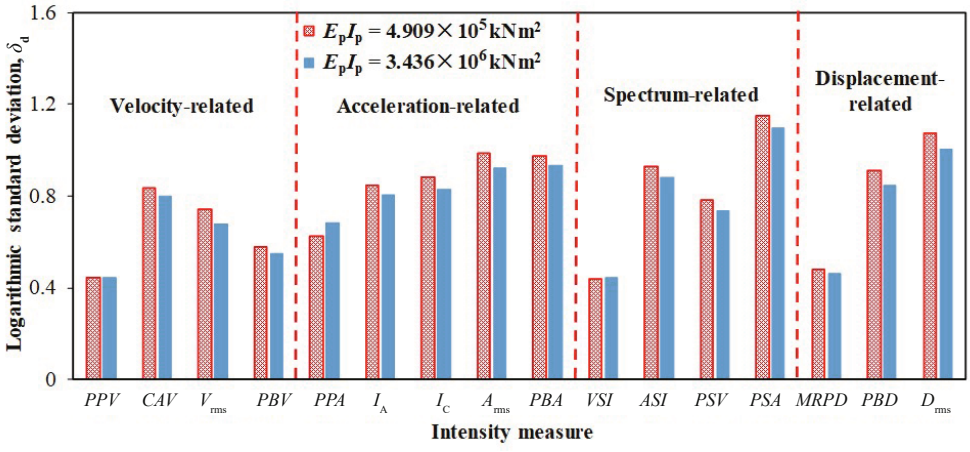

(b) Pile

Fig. 11 Comparison of the logarithmic standard deviations for the curvature ductility of piled pier system employing different ground motion intensity measures (notations are consistent with those listed in Table 4)

section, seismic fragility analysis is subsequently performed on the clay-pile-superstructure system. In the fragility analysis, the probability of a structural demand surpassing one damage state is expressed as follows.

$$P_{\mathrm{f}} = P[S_{\mathrm{d}} \geq S_{\mathrm{c}}] \tag{8}$$

where P_{f} is the probability of a structural demand surpassing one damage state; P represents the probability of an event; and S_{c} is the structural capacity, characterized by the four damage states as listed in Table 3.

The seismic structural demand and capacity are generally considered to follow lognormal distributions. Hence, Eq. (8) can be converted into the following expression:

$$P_{\mathrm{f}} = P[S_{\mathrm{d}} \geq S_{\mathrm{c}}] = P[\ln(S_{\mathrm{d}}) - \ln(S_{\mathrm{c}}) \geq 0] = \Phi\left[\frac{\ln(S_{\mathrm{d}}/S_{\mathrm{c}})}{\sqrt{\delta_{\mathrm{d}}^2 + \delta_{\mathrm{c}}^2}}\right] \tag{9}$$

where δ_{c} is the logarithmic standard deviation for the structural capacity; and Φ is the standard normal distribution function.

In the present study, only the uncertainty in structural demand is taken into consideration. Combining Eqs. (7) and (9) leads to

$$P_{\mathrm{f}} = \Phi\left[\frac{\ln(S_{\mathrm{d}}/S_{\mathrm{c}})\sqrt{N-2}}{\sqrt{\sum_{i=1}^{N}\left\{\ln(S_{\mathrm{d}i}) - \left[b\ln(IM_i) + a\right]\right\}^2}}\right] \tag{10}$$

5.1 Influence of bridge superstructure mass

To explore the influence of the inertial effect on the seismic damage degree of the piled pier system, three added masses, namely 100 t, 320 t and 960 t, are employed to represent different bridge girder masses, while the pile flexural rigidity is kept as 1.473×10^6 kN·m^2.

Following the framework of Eq. (6), Fig. 12 shows the plots of pier curvature ductility against PPA on a logarithmic scale involving three different added masses, along with the best-fit lines. As can be seen, the pier ductility tends to significantly increase with the increasing PPA, which is partly the reason why the logarithmic standard deviation becomes more evidently associated with the added mass of 960 t.

On the other hand, Fig. 13 shows that the pile ductility versus PPV data sets involving different added masses can generally be well represented by the respective best-fit lines; different from the trends shown in Fig. 12, the increasing trend of pile curvature ductility versus added mass is relatively mild, indicating that the seismic pile response is predominantly dependent on the kinematic force arising from the surrounding soils.

The regressed parameters shown on Figs. 12 and 13 can be substituted into the Eq. (10), and a suite of seismic fragility curves for both the pier and the pile corresponding to four different damage states can be established. As can be seen from Fig. 12, for the three added masses considered, evident damage to the pier occurs only for added mass equal to 960 t. Hence, only the seismic fragility curves for the pier pertaining to added mass of 960 t are presented in Fig. 14.

As Fig. 14 shows, the damage probability of the pier increases gradually with the increasing PPA, disregarding the damage states. When the PPA is less than 0.1 g, the damage probability of the pier is hardly seen, indicating that it generally behaves within the elastic domain, which is consistent with the trend shown in Fig. 7(b). In addition, for the ground motion intensities considered in this study, the pier is not likely to experience "complete damage" as its maximum probability to exceed this damage state is less than 2%.

As Fig. 15 shows, the damage probabilities of the pile clearly augment with the increasing PPV, regardless of the added masses employed. In addition, the increase

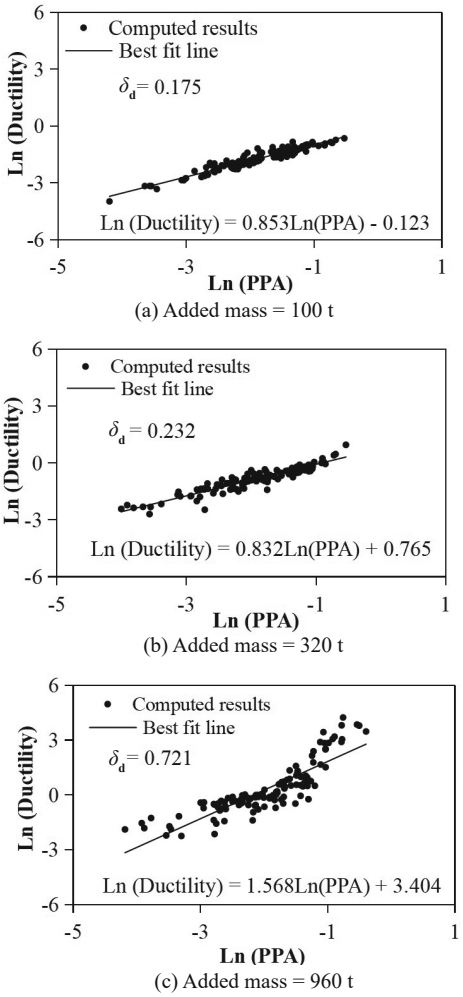

Fig. 12 Regression between ground motion intensity and curvature ductility for pier with varying added masses (pile flexural rigidity $E_{\mathrm{p}}I_{\mathrm{p}} = 1.473\times10^6$ kN·m^2)

in bridge girder mass tends to aggravate the seismic damage of pile, especially for exceeding extensive to complete damage extents.

5.2 Influence of pile flexural rigidity

Pile flexural rigidity varies within a large range due to the difference in pile diameter and/or pile material employed in engineering practice, which is a crucial factor affecting the seismic performance of a pile-soil system. In this subsection, three pile flexural rigidities, namely 4.909×10^5 kN·m^2, 1.473×10^6 kN·m^2, and 3.436×10^6 kN·m^2 were considered, while the bridge girder mass is maintained at 320 t. As can be seen from Figs. 16 and 12(b), there is a slightly decreasing trend of pier curvature ductility against pile flexural rigidity; In addition, for the adopted 120 ground motions and added mass equal to 320 t, the pier curvature ductility values are generally less than 1, indicating that the pier is not likely to experience severe seismic damage. As a result, the relevant pier fragility curves are not necessary.

In contrast, as Figs. 17 and 13(b) indicate, with the augmented pile flexural rigidity, the pile curvature has a decreasing trend. For example, for PPV equal to 0.4 m/s, the pile curvature ductility values are, on average, 4.2, 3.6 and 2.9 for pile flexural rigidities equal to 4.909×10^5 kN·m^2, 1.473×10^6 kN·m^2 and 3.436×10^6 kN·m^2, respectively.

The seismic fragility curves of the pile with different flexural rigidities are presented in Fig. 18, which shows that, as the pile flexural rigidity increases, the failure probabilities of the pile clearly become smaller,

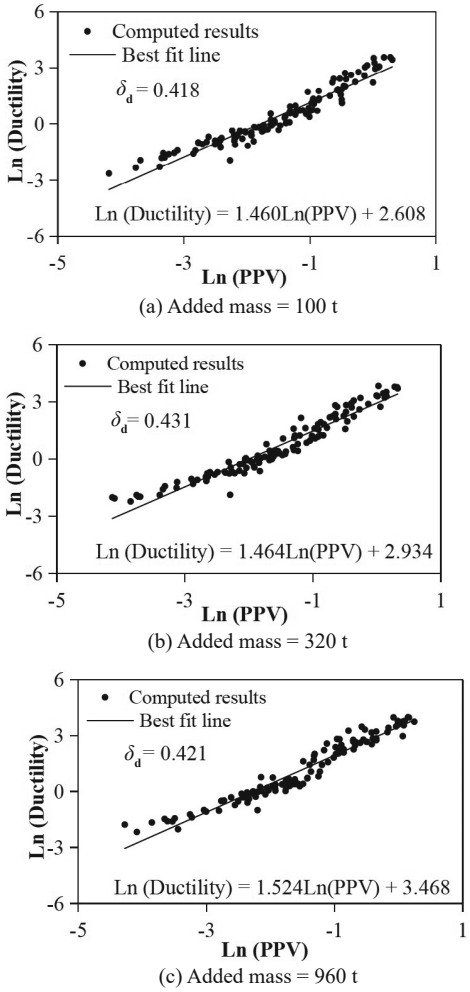

Fig. 13 Regression between ground motion intensity and curvature ductility for pile involving different added masses ($E_pI_p = 1.473\times10^6$ kN·m^2)

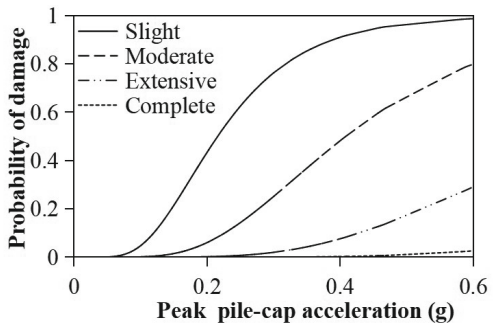

Fig. 14 Pier fragility curves pertaining to different extents of damage ($E_pI_p = 1.473\times10^6$ kN·m^2, added mass = 960 t)

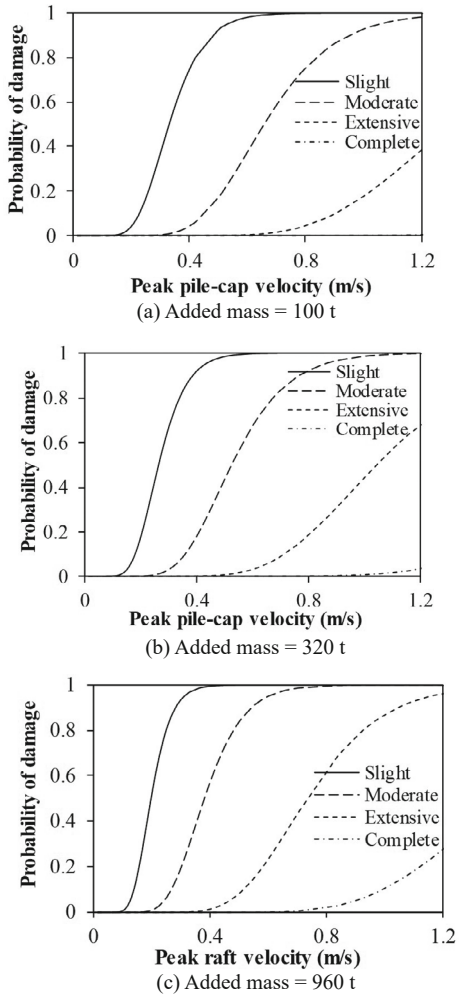

Fig. 15 Pile fragility curves pertaining to different damage extents and varying added masses ($E_pI_p = 1.473\times10^6$ kN·m^2)

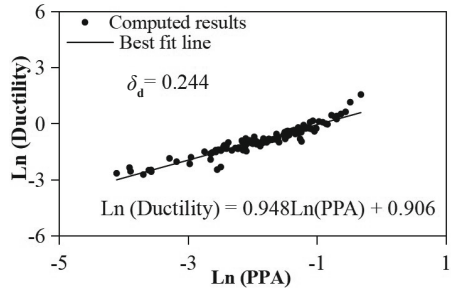

(a) $E_pI_p = 4.909\times10^5$ kN·m^2

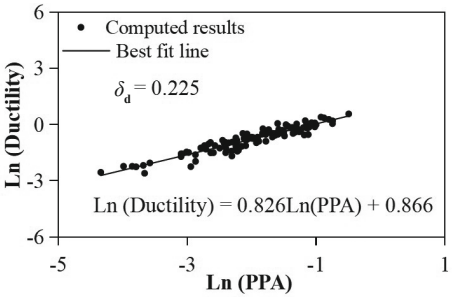

(b) $E_pI_p = 3.436\times10^6$ kN·m^2

Fig. 16 Regression between ground motion intensity and curvature ductility for pier with different pile flexural rigidities (added mass = 320 t)

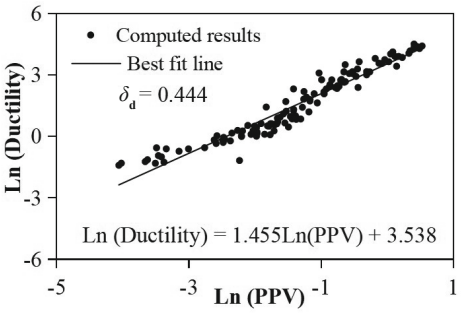

(a) $E_pI_p = 4.909\times10^5$ kN·m^2

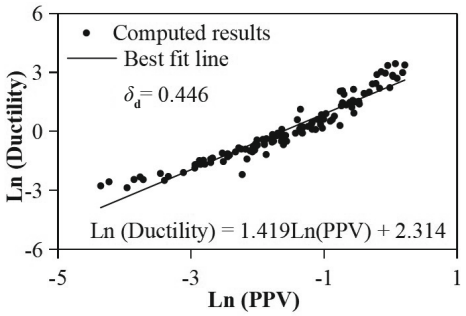

(b) $E_pI_p = 3.436\times10^6$ kN·m^2

Fig. 17 Regression between ground motion intensity and curvature ductility for pile with different pile flexural rigidities (added mass = 320 t)

disregarding the damage states. For PPV equal to 0.4 m/s, the probabilities of exceeding a moderate damage extent are 70%, 17% and 1% for pile flexural rigidities equal to 4.909×10^5 kN·m^2, 1.473×10^6 kN·m^2 and 3.436×10^6 kN·m^2, respectively, suggesting that the seismic capacity of the pile can be significantly increased by increasing the pile flexural rigidity.

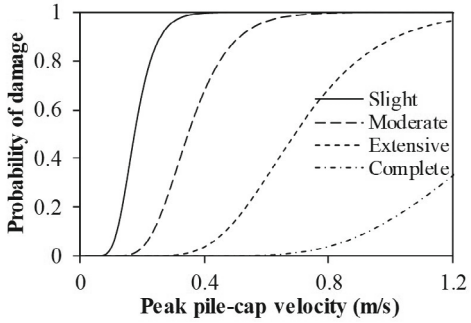

(a) $E_pI_p = 4.909\times10^5$ kN·m^2

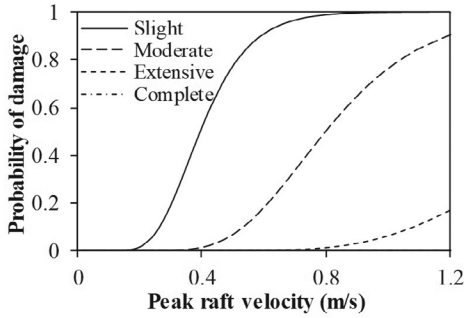

(b) $E_pI_p = 3.436\times10^6$ kN·m^2

Fig. 18 Pile fragility curves pertaining to different damage extents and different pile flexural rigidities (added mass = 320 t)

6 Conclusions

In this study, a series of FE dynamic analyses were carried out to explore the seismic performance of a clay-pile-pier system subjected to 120 realistic ground motions, with the consideration of variations in both pile flexural rigidity and bridge superstructure mass. The focus of the investigation was placed on the maximum seismic bending behavior of both the pier and the pile, while the curvature ductility was employed to quantify the seismic damage extents of the system. Comprehensive comparison studies were performed to obtain the corresponding optimal ground motion intensity measures for evaluating the seismic responses of the pile and the pier, respectively. Furthermore, seismic fragility curves of both the pier and the pile with respect to various damage states were established. The following main conclusions can be drawn:

(1) Due to the nonlinear dynamic behavior of clay and the complexity in seismic soil-pile interaction, both the maximum curvature and bending moment responses of the piled pier system appear to nonlinearly vary against the ground motion intensity, generally with increasing trends to varying degrees. For strong ground motions with PBA > 0.15 g or PPV > 0.25 m/s, the maximum bending moment of the pile becomes almost unchanged, while the maximum curvature of pile continues to monotonically increase against the ground motion intensity as shown in Fig. 9. Hence, the maximum curvature response is comparatively more viable for characterizing the seismic damage evolution process of the piled pier system.

(2) A series of comparison studies involving 16 ground motion intensity measures suggest that the seismic response of the pile-pier system is most dependent on the foundation-level (i.e., pile cap) ground motion intensity; for the evaluation of the seismic performance of the pile-pier system, PPA and PPV are found to be the optimal ground motion intensity measures for the pier and the pile, respectively.

(3) With the augment in bridge girder mass, the seismic response of the pier has a clear increasing trend, while such an increasing trend is not evident for pile. On the other hand, the pile flexural rigidity tends to have a more pronounced influence on the seismic response of the pile rather than that of the pier. This suggests that the seismic responses of the pier and the pile are more dependent on the inertial force arising from the bridge superstructure and kinematic force imposed by the surrounding soils, respectively. Furthermore, as compared to the pier, the pile is more vulnerable to earthquake-induced damage, which can be effectively alleviated by increasing the pile flexural rigidity.

On the basis of optimal ground motion intensity measures observed in this study, the fragility curves and regressed correlations presented are more viable for preliminarily evaluating the seismic damage risk of a piled pier system built in soft clayey strata. However, the findings obtained in this study can be further refined as and when more results from both numerical and experimental studies are available.

Acknowledgment

The authors greatly acknowledge the financial support provided by the National Natural Science Foundation of China (Grant Nos. 52178353, 51808421) and the Fundamental Research Funds for the Central Universities (WUT: 2020III043).

References

Azizkandi AS, Baziar MH and Yeznabad AF (2018), "3D Dynamic Finite Element Analyses and 1 g Shaking Table Tests on Seismic Performance of Connected and Nonconnected Piled Raft Foundations," *KSCE Journal of Civil Engineering*, **22**(5): 1750–1762.

Banerjee S, Goh SH and Lee FH (2014), "Earthquake-Induced Bending Moment in Fixed-Head Piles in Soft Clay," *Géotechnique*, **64**(6): 431–446.

Bhattacharya S, Tokimatsu K, Goda K, Sarkar R, Shadlou M and Rouholamin M (2014), "Collapse of Showa Bridge During 1964 Niigata Earthquake: A Quantitative Reappraisal on the Failure Mechanisms," *Soil Dynamics and Earthquake Engineering*, **65**: 55–71.

Boulanger RW, Curras CJ, Kutter BL, Wilson DW and Abghari A (1999), "Seismic Soil-Pile-Structure Interaction Experiments and Analyses," *Journal of Geotechnical and Geoenvironmental Engineering*, **125**(9): 750–759.

Bradley BA, Cubrinovski M, Dhakal RP and Macrae GA (2009), "Intensity Measures for the Seismic Response of Pile Foundations," *Soil Dynamics and Earthquake Engineering*, **29**(6): 1046–1058.

Brandenberg SJ, Kashighandi P, Zhang J, Huo Y and Zhao M (2011), "Fragility Functions for Bridges in Liquefaction-Induced Lateral Spreads," *Earthquake Spectra*, **27**(3): 683–717.

Chen LW, Wu XY and Tang C (2022), "Simplified Prediction Method for PGA Amplification Factors Corrected by Site Conditions," *Journal of Southwest Jiaotong University*, **57**(1): 173–181. (in Chinese)

Choi ES, Desroches R and Nielson B (2004), "Seismic Fragility of Typical Bridges in Moderate Seismic Zones," *Engineering Structures*, **26**(2): 187–199.

Cornell AC, Jalayer F and Hamburger RO (2002), "Probabilistic Basis for 2000 SAC Federal Emergency Management Agency Steel Moment Frame Guidelines," *Journal of Structural Engineering*, **128**(4): 526–532.

Dehghanpoor A, Thambiratnam D, Taciroglu E and Chan T (2019), "Soil-Pile-Superstructure Interaction Effects in Seismically Isolated Bridges Under Combined Vertical and Horizontal Strong Ground Motions," *Soil Dynamics and Earthquake Engineering*, **126**: 105753.

Drygala IJ, Dulinska JM and Wazowski M (2017), "Seismic Performance of a Cable-Stayed Footbridge Using a Concrete Damage Plasticity Model," *Procedia Engineering*, **193**: 525–532.

GB 50011-2010 (2010), *Code for Seismic Design of Buildings*, Beijing: China Architecture and Building Press. (in Chinese)

Hwang H, Jernigan JB and Lin YW (2000), "Evaluation of Seismic Damage to Memphis Bridges and Highway Systems," *Journal of Bridge Engineering*, **5**(4): 322–330.

Jankowiak T and Łodygowski T (2005), "Identification of Parameters of Concrete Damage Plasticity Constitutive Model," *Foundation of Civil and Environmental Engineering*, **6**(1): 53–69.

Li YR, Zhang J, Chen HB, Qiang DF and Wang YZ (2022), "Study on the Dynamic Response Characteristics and p–y Curve of Straight and Inclined Pile Groups in Saturated Sands," *Applied Sciences*, **12**(5): 2363.

Maheshwari BK, Truman KZ, El Naggar MH and Gould PL (2004), "Three-Dimensional Nonlinear Analysis for Seismic Soil-Pile-Structure Interaction," *Soil Dynamics and Earthquake Engineering*, **24**(4): 343–356.

Mayoral JM, Alberto Y, Mendoza MJ and Romo MP (2009), "Seismic Response of an Urban Bridge-Support System in Soft Clay," *Soil Dynamics and Earthquake Engineering*, **29**(5): 925–938.

Meymand PJ (1998), "Shaking Table Scale Model Test of Nonlinear Soil-Pile-Superstructure Interaction in Soft

Clay," *PhD Thesis*, Berkeley: University of California, Berkeley, USA.

Mohanty P, Xu D, Biswal S and Bhattacharya S (2021), "A Shake Table Investigation of Dynamic Behavior of Pile Supported Bridges in Liquefiable Soil Deposits," *Earthquake Engineering and Engineering Vibration*, **20**(1): 1–24.

Mylonakis G, Syngros C, Gazetas G and Tazoh T (2006), "The Role of Soil in the Collapse of 18 Piers of Hanshin Expressway in the Kobe Earthquake," *Earthquake Engineering and Structural Dynamics*, **35**(5): 547–575.

Riddell R (2007), "On Ground Motion Intensity Indices," *Earthquake Spectra*, **23**(1): 147–173.

Padgett JE, Nielson BG and DesRoches R (2008), "Selection of Optimal Intensity Measures in Probabilistic Seismic Demand Models of Highway Bridge Portfolios," *Earthquake Engineering and Structural Dynamics*, **37**(5): 711–725.

Saha R, Haldar S and Dutta SC (2015), "Influence of Dynamic Soil-Pile Raft-Structure Interaction: An Experimental Approach," *Earthquake Engineering and Engineering Vibration*, **14**(4): 625–645.

Shafieezadeh A, Ramanathan K, Padgett JE and DesRoches R (2012), "Fractional Order Intensity Measures for Probabilistic Seismic Demand Modeling Applied to Highway Bridges," *Earthquake Engineering and Structural Dynamics* **41**(3): 391–409.

Song S, Qian C, Qian YJ, Bao H and Lin PZ (2019), "Canonical Correlation Analysis of Selecting Optimal Ground Motion Intensity Measures for Bridges," *KSCE Journal of Civil Engineering*, **23**(7): 2958–2970.

Tang C and Chen LW (2020), "Probability Modelling of PGA Amplification Factors Corrected by Site Conditions," *Engineering Mechanics*, **37**(12): 99–113. (in Chinese)

Tang L, Ling XZ, Xu PJ, Gao X and Wang DS (2010), "Shake Table Test of Soil-Pile Groups-Bridge Structure Interaction in Liquefiable Ground," *Earthquake Engineering and Engineering Vibration*, **9**(1): 39–50.

Tang L, Zhang XY, Ling XZ, Li H and Ju NP (2016), "Experimental and Numerical Investigation on the Dynamic Response of Pile Group in Liquefying Ground," *Earthquake Engineering and Engineering Vibration*, **15**(1): 103–114.

Tavares DH, Suescun JR, Paultre P and Padgett JE (2013), "Seismic Fragility of a Highway Bridge in Quebec," *Journal of Bridge Engineering*, **18**(11): 1131–1139.

Tinawi R, Sarrazin M and Filiatrault A (1993), "Influence of Soft Clays on the Response Spectra for Structures in Eastern Canada," *Soil Dynamics and Earthquake Engineering*, **12**(8): 469–477.

Tsinidis G, Rovithis E, Pitilakis K and Chazelas JL (2016), "Seismic Response of Box-Type Tunnels in Soft Soil: Experimental and Numerical Investigation," *Tunnelling and Underground Space Technology*, **59**: 199–214.

Wang QA, Wu ZY and Liu SK (2012), "Seismic Fragility Analysis of Highway Bridges Considering Multi-Dimensional Performance Limit State," *Earthquake Engineering and Engineering Vibration*, **11**(2): 185–193.

Wang X, Ye A and Ji B (2019), "Fragility-Based Sensitivity Analysis on the Seismic Performance of Pile-Group-Supported Bridges in Liquefiable Ground Undergoing Scour Potentials," *Engineering Structures*, **198**: 109427.

Wu XY, Chen LW and Yuan XM (2021), "Characteristics of Long-Period Displacement Spectra Based on Strong Ground-Motion Records," *Journal of Building Structures*, **42**(5): 195–205. (in Chinese)

Yakhchalian M, Nicknam A and Amiri GG (2015), "Optimal Vector-Valued Intensity Measure for Seismic Collapse Assessment of Structures," *Earthquake Engineering and Engineering Vibration*, **14**(1): 37–54.

Yang CSW, Werner SD and DesRoches R (2015), "Seismic Fragility Analysis of Skewed Bridges in The Central Southeastern United States," *Engineering Structures*, **83**(1): 116–128.

Yang J, Yang M and Chen HB (2019), "Influence of Pile Spacing on Seismic Response of Piled Raft in Soft Clay: Centrifuge Modeling," *Earthquake Engineering and Engineering Vibration*, **18**(4): 719–733.

Yang M and Yang J (2016), "Centrifuge Tests on Seismic Response of Piled Raft Foundation with Large Spacing," *Chinese Journal of Geotechnical Engineering*, **38**(12): 2184–2193. (in Chinese)

Zelaschi C, Monteiro R and Pinho R (2019), "Critical Assessment of Intensity Measures for Seismic Response of Italian RC Bridge Portfolios," *Journal of Earthquake Engineering*, **23**(6): 980–1000.

Zhang J, Huo Y, Brandenberg SJ and Kashighandi P (2008), "Effects of Structural Characterizations on Fragility Functions of Bridges Subject to Seismic Shaking and Lateral Spreading," *Earthquake Engineering and Engineering Vibration*, **7**(4): 369–382.

Zhang J, Li YR, Yan ZX, Huang D, Rong X and Liang Y (2022), "Experimental Study of Vertical and Batter Pile Groups in Saturated Sand Using a Centrifuge Shaking Table," *Earthquake Engineering and Engineering Vibration*, **21**(1): 23–36.

Zhang L, Goh SH and Liu HB (2017a), "Seismic Response of Pile-Raft-Clay System Subjected to a Long-Duration Earthquake: Centrifuge Test and Finite Element Analysis," *Soil Dynamics and Earthquake Engineering*, **92**: 488–502.

Zhang L, Goh SH and Yi JT (2017b), "A Centrifuge Study of the Seismic Response of Pile-Raft Systems Embedded in Soft Clay," *Géotechnique*, **67**(6): 479–490.

Zhang L and Liu HB (2017), "Seismic Response of Clay-Pile-Raft-Superstructure Systems Subjected to Far-

Field Ground Motions," *Soil Dynamics and Earthquake Engineering*, **101**: 209–224.

Zhang L, Zhang PP, Xu DS and Zhou T (2021), "Seismic Damage Analysis of Piled Pier System Constructed on Soft Clay Ground," *Journal of Bridge Engineering*, **26**(3): 04020133.

Zhong J, Jeon JS, Shao YH and Chen L (2019), "Optimal Intensity Measures in Probabilistic Seismic Demand Models of Cable-Stayed Bridges Subjected to Pulse-Like Ground Motions," *Journal of Bridge Engineering*, **24**(2): 04018118.1–17.

Zhong J, Pang YT and Yuan WC (2016), "Evaluation of Optimal Intensity Measures in Fragility Analysis of Cable-Stayed Bridges," *Journal of Tongji University* (*Natural Science*), **44**(9): 1340–1346, 1370. (in Chinese)